Very low excess noise $Al_{0.75}Ga_{0.25}As_{0.56}Sb_{0.44}$ avalanche photodiode

XIAO JIN,[1,†] **HARRY I. J. LEWIS,[1,2,†]** **XIN YI,[3]** **SHIYU XIE,[4,5]**
BAOLAI LIANG,[6,8] **QINGYU TIAN,[1]** **DIANA L. HUFFAKER,[3,4,7]**
CHEE HING TAN,[1] **AND JOHN P. R. DAVID[1,9]**

[1]*Department of Electronic and Electrical Engineering, University of Sheffield, Sheffield, S1 3JD, UK*
[2]*Currently with: TRIUMF, 4004 Westbrook Mall, Vancouver, BC, V6T 2A3, Canada*
[3]*Institute of Photonics and Quantum Sciences, School of Engineering and Physical Sciences, Heriot-Watt University, David Brewster Building, Edinburgh, EH14 4AS, UK*
[4]*School of Physics and Astronomy, Cardiff University, Queen's Building, The Parade, Cardiff, CF24, UK*
[5]*Microsemi Ltd., Shanghai, 200001, China*
[6]*California NanoSystems Institute, University of California, Los Angeles, California, 90095, USA*
[7]*Electrical Engineering Department, The University of Texas at Arlington, Texas, 76019, USA*
[8]*bliang@cnsi.ucla.edu*
[9]*j.p.david@sheffield.ac.uk*
[†]*These authors contributed equally.*

Abstract: $Al_xGa_{1-x}As_ySb_{1-y}$ grown lattice-matched to InP has attracted significant research interest as a material for low noise, high sensitivity avalanche photodiodes (APDs) due to its very dissimilar electron and hole ionization coefficients, especially at low electric fields. All work reported to date has been on Al concentrations of $x = 0.85$ or higher. This work demonstrates that much lower excess noise ($F = 2.4$) at a very high multiplication of 90 can be obtained in thick $Al_{0.75}Ga_{0.25}As_{0.56}Sb_{0.44}$ grown on InP substrates. This is the lowest excess noise that has been reported in any III-V APD operating at room temperature. The impact ionization coefficients for both electrons and holes are determined over a wide electric field range (up to 650 kV/cm) from avalanche multiplication measurements undertaken on complementary *p-i-n* and *n-i-p* diode structures. While these ionization coefficients can fit the experimental multiplication over three orders of magnitude, the measured excess noise is significantly lower than that expected from the β/α ratio and the conventional local McIntyre noise theory. These results are of importance not just for the design of APDs but other high field devices, such as transistors using this material.

1. Introduction

There is significant interest in LiDAR systems for applications ranging from space-borne instruments for greenhouse gas emissions to accurate 3D sensing and mapping in urban environments for next-generation fully autonomous vehicles [1,2]. For these photon-starved applications, the detector requirements can be fulfilled by avalanche photodiodes (APDs). These can provide higher sensitivity than conventional *p-i-n* diodes due to their internal multiplication, which is provided by the process of impact ionization [3]. However, the stochastic nature of this process results in an excess noise factor (F), which increases with multiplication as described by McIntyre's local field theory [4]:

$$F = kM + \left(2 - \frac{1}{M}\right)(1 - k) \tag{1}$$

Where M is the device multiplication factor and $k = \beta/\alpha$, with β and α denoting the impact ionization coefficients for holes and electrons respectively. The value of F limits the maximum multiplication achievable while maintaining a large signal to noise ratio (SNR), necessitating the use of avalanche materials with a small k. A small k reduces the effects of carrier feedback in impact ionization. This results in lower noise and improved bandwidth [5]. Since the α and β in most semiconductors tend to become similar as the electric field increases, low noise APDs have tended to have thick avalanching regions to allow operation at lower electric fields.

While silicon has excellent excess noise properties due to its small k, it is not able to detect photons beyond 1000 nm [6] and attempts to integrate it with a Ge absorber result in high dark currents and a poor quantum efficiency [7–9]. APDs capable of operating at telecommunications wavelengths of 1550 nm have therefore relied on a narrow band gap InGaAs absorber and a wider band gap multiplication layer, all grown lattice-matched on an InP substrate. These are incorporated into a separate absorption, charge and multiplication (SACM) heterojunction configuration with a low electric field in the absorber to reduce the tunnelling current and a high electric field in the multiplication region to provide the gain. The InP or InAlAs commonly used as the multiplication region in these structures however has excess noise that is fairly high [10,11] due to the similar values of α and β. Low noise APDs capable of operating at 1550 nm have been demonstrated by the use of narrow band gap materials such as HgCdTe [12–14] and InAs [15], but these tend to require cooling to reduce the dark currents. $Al_xIn_{1-x}AsSb$ grown lattice-matched to GaSb has demonstrated excellent APD performance at room temperature with absorption that extends beyond 1500 nm [16–18], but requires more complicated growth techniques and is not compatible with a conventional InP based photonics platform. In the last few years, $Al_xGa_{1-x}As_ySb_{1-y}$ has established itself as a significantly better low noise multiplication material than InP and InAlAs as it can also be grown lattice-matched to InP and combined with an InGaAs [19,20] or GaAsSb [21–23] absorption layer.

Research into the ionization properties of $Al_xGa_{1-x}As_ySb_{1-y}$ has so far has been limited to high-Al alloys with x of 1.0 - 0.85. Initial work by Yi *et al.* on AlAsSb showed that β was much lower than α [24], corresponding to extremely low excess noise equivalent to a k value of 0.005 in a 1550 nm *p-i-n* structure [25]. However, the high Al content of these alloys resulted in high surface leakage dark current and poor device reliability due to surface oxidation. $Al_{0.85}Ga_{0.15}As_{0.56}Sb_{0.44}$ does not oxidize as readily, and Lee *et al.* showed that nominally 1000 nm avalanching region *p-i-n* structures grown as a digital alloy (DA) and random alloy (RA) showed low excess noise behavior with $k = 0.01$ [26] and $k = 0.02$ [27] respectively. Even thinner 600 nm avalanching region $Al_{0.85}Ga_{0.15}As_{0.5\ 6}Sb_{0.44}$ *p-i-n* diodes have shown relatively low noise in this alloy system [28,29]. Extraction of the ionization coefficients in this material over a wide electric field range [30] showed that the α remained the same as that of AlAsSb at low electric field but that β had increased slightly. There are a number of reasons why an even lower Al composition alloy multiplication region may be better. The grading scheme from the InGaAs or GaAsSb absorber to the $Al_{0.85}Ga_{0.15}As_{0.56}Sb_{0.44}$ multiplication region can be complicated due to the large conduction band discontinuity, so using $Al_xGa_{1-x}As_ySb_{1-y}$ with lower Al content as the multiplication region would be beneficial. Further decreasing Al content may also mitigate the effects of oxidation and high surface leakage currents and reduce the operating voltage of the APD. This study investigates the impact ionization characteristics of complementary *p-i-n* and *n-i-p* structures of $Al_{0.75}Ga_{0.25}As_{0.56}Sb_{0.44}$ (hereafter $Al_{0.75}Ga_{0.25}AsSb$). Multiplication has been measured under pure electron (M_e) and pure hole (M_h) injection conditions for the *p-i-n* and *n-i-p* structures respectively. Impact ionization coefficients are determined from the multiplication measurements using a 'local' model [31], where the carrier ionization probability for a given position within a device is assumed to be only a function of the electric field at that point, and no allowance is made for any 'dead-space' or history dependence of the carrier energy [32]. The dark currents and excess noise characteristics are reported for this alloy composition

for the first time. This work provides important information on the $Al_xGa_{1-x}As_ySb_{1-y}$ alloy system, which will inform the design of high-performance SWIR APDs. While APDs require information about the ionization behaviour at high multiplication values, other devices such as high frequency double heterojunction bipolar transistors (DHBTs) on InP are also likely to benefit from an accurate understanding of this behaviour at low electric fields [33].

2. Wafer details

The $Al_{0.75}Ga_{0.25}AsSb$ homojunction *p-i-n* and *n-i-p* structures (P1 and N1 respectively) are shown schematically in Fig. 1(a) with p^+ and n^+ cladding layer dopings of $\sim 2 \times 10^{18} cm^{-1}$ and thicknesses of 300 nm. The unintentionally doped intrinsic regions were nominally 1500 nm thick. Growth was undertaken at a temperature of 500°C on epi-ready n^- InP (001) (*p-i-n* structure) and p^- InP (001) (*n-i-p* structure) substrates, in a Veeco GEN930 MBE reactor where both As_2 and Sb_2 fluxes are supplied using valved cracker cells. The $Al_{0.75}Ga_{0.25}AsSb$ was grown as a short period superlattice (~ 1.3 nm period) with rapidly alternating layers of AlGaAs (0.17 nm) and AlGaSb (1.13 nm) in order to meet the conditions of lattice-matching. Further details of this digital growth technique can be found in Yi *et al.* [24]. The wafers also had highly doped 20 nm top and 400 nm bottom InGaAs contact layers. Mesa diodes of 90, 140, 240, and 440 μm
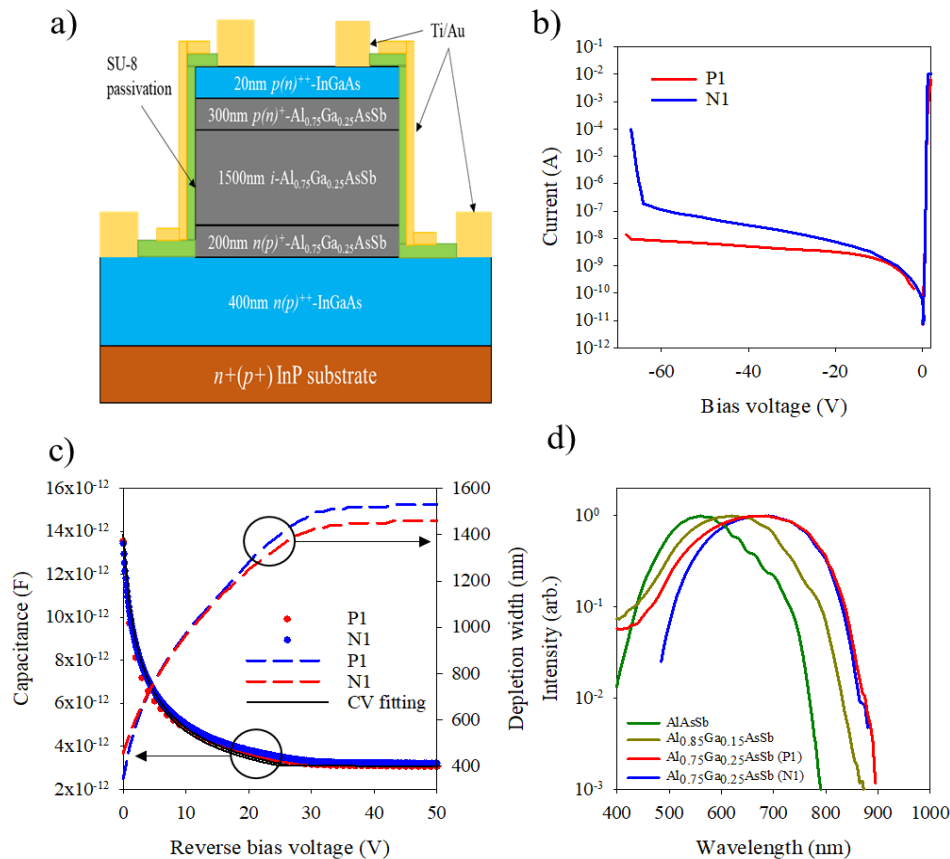

Fig. 1. a) A schematic diagram of P1 and N1. b) Forward and reverse bias dark current data for P1 and N1 for 240 μm diameter devices. c) Capacitance-voltage data for 240 μm diameter devices. d) Photocurrent spectra for P1 and N1 compared to those for $Al_{0.85}Ga_{0.15}As_{0.56}Sb_{0.44}$ and AlAsSb.

diameter with annular optical windows were fabricated using standard wet etching in a solution composed of [1 ml HCl]: [8 ml H_2O_2]: [80 ml H_2O]. Ti/Au was used for the top and bottom metal contacts. The mesa sidewalls were passivated with SU-8 and coated with gold to prevent light from falling on them.

3. Experimental methods and results

In Fig. 1(b), forward current-voltage (I-V) measurements show negligible series resistance and scaled with area with an ideality factor of ~1.8 at high bias. However, the reverse dark currents for both P1 and N1 scaled with device perimeter, indicating that surface leakage effects dominate, and that the bulk dark currents are significantly lower. The breakdown voltages for P1 (69 V) and N1 (68 V) were similar.

Capacitance-voltage (C-V) measurements were performed at a frequency of 1 MHz using an HP4275 LCR meter. Device region widths and dopings were extracted from these and using a dielectric constant of 11.7, interpolated from those of AlAsSb [24] and GaAsSb [34], giving intrinsic region (*i*-region) thicknesses of 1500 nm (P1) and 1440 nm (N1) with a background doping of 1.5×10^{16} cm^{-3} for both structures. This small difference in thickness accounts for the difference in breakdown voltage between P1 and N1. As shown in Fig. 1(c), the capacitance decreases significantly with reverse bias up to approximately 30 V, indicating that the *i*-regions of the structures are not fully depleted before this point. The capacitance changes very little once the depletion reaches the heavily doped cladding layers. The wavelength dependent photocurrent spectra for P1 and N1 were measured using a tungsten halogen bulb and a monochromator (Fig. 1(d)) at a reverse bias voltage at which the *i*-regions were just fully depleted. This data confirms the expected decrease of the band gap with decreasing Al content from the change in the absorption cut-off compared to reports in the literature [35] and with measurements undertaken on a 1550 nm thick homojunction AlAsSb *p-i-n* from Yi *et al.* [25]. P1 and N1 have a similar cutoff at ~870 nm suggesting that the alloy compositions are identical, however P1 has a higher short wavelength response. This is presumably due to the longer electron diffusion lengths (L_e) in the top p^+ doped cladding layer, relative to the minority hole diffusion length in the top n^+ layer in N1.

Figure 2(a) shows photocurrent versus reverse bias voltage for P1 and N1 undertaken with light from a fibre-coupled 455 nm LED. These measurements were performed using a phase sensitive technique to remove the contribution of any DC dark currents. This wavelength ensures 'pure' injection conditions, where more than 99% of photogenerated carriers are generated in the top p^+ (n^+) cladding layers and only electrons (holes) diffuse into the high electric field avalanching region in the *p-i-n* and *n-i-p* structures respectively. The photocurrent in the *p-i-n* increases rapidly initially with reverse bias unlike that in the *n-i-p*, leading us to conclude that the background doping in the intrinsic region is *p*-type, similar to that seen in higher Al compositions [24]. The movement of the depletion edge with bias towards the source of optically generated carriers can lead to an increasing photocurrent [36]. The challenge in the *p-i-n* structure is to separate the increase in photocurrent due to electron-initiated multiplication (M_e) from this other mechanism. The movement of the depletion edge with bias is much less significant in the *n-i-p* structure and this can be easily corrected for using a simple linear fit [36], allowing hole-initiated multiplication (M_h) to be accurately determined.

In order to simulate the bias dependent photocurrent, we require information about the minority carrier diffusion lengths for electrons (L_e) and holes (L_h), the rate of movement of the depletion edge and the ionization coefficients α and β. The photocurrent of the structure shown in Fig. 1(a) was simulated using a Silvaco TCAD model with the absorption coefficient of the 455 nm light (γ), L_e, L_h, α and β used as fitting parameters until good agreement with the experimentally measured photocurrent shown in Fig. 2(a) could be obtained. The red line in Fig. 2(a) shows
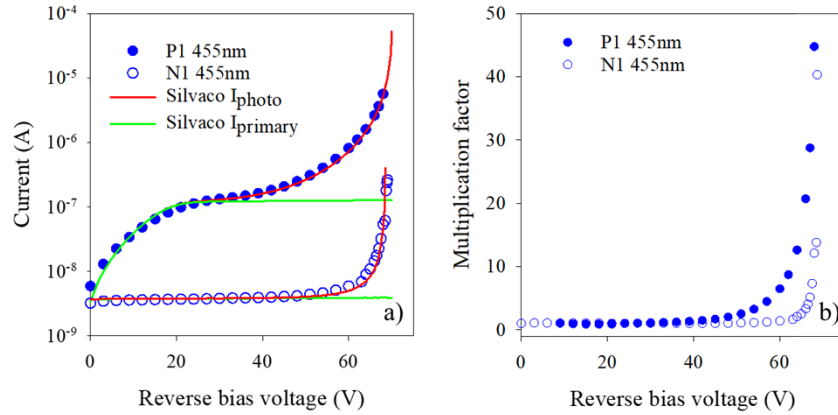
Fig. 2. a) P1 and N1 photocurrent under 455 nm illumination, shown with Silvaco TCAD simulation of the primary and multiplied photocurrents. b) Multiplication factor versus reverse bias voltage for P1 and N1 under 455 nm illumination.

that the simulated photocurrent using $\gamma = 1.5 \times 10^5 \, \text{cm}^{-1}$, $L_e = 264 \, \text{nm}$, $L_h = 100 \, \text{nm}$ and impact ionization coefficients given by the Chynoweth expressions [37] in Eqs. (2) and (3) gives excellent agreement with experimental measurements from 0 V to 70 V.

$$\alpha = \begin{cases} 6.87 \times 10^5 \exp\left(-\left(\frac{1.21 \times 10^6}{E}\right)^{1.43}\right) \text{cm}^{-1} \\ \qquad \text{when } E < 500 kV/cm \\ 10.0 \times 10^5 \exp\left(-\left(\frac{1.30 \times 10^6}{E}\right)^{1.43}\right) \text{cm}^{-1}, \\ \qquad \text{when } 500 kV/cm < E < 650 kV/cm \end{cases} \qquad (2)$$

$$\beta = \begin{cases} 3.12 \times 10^5 \exp\left(-\left(\frac{1.70 \times 10^6}{E}\right)^{1.44}\right) \text{cm}^{-1}, \\ \qquad \text{when } E < 500 kV/cm \\ 5.62 \times 10^5 \exp\left(-\left(\frac{1.92 \times 10^6}{E}\right)^{1.38}\right) \text{cm}^{-1}, \\ \qquad \text{when } 500 kV/cm < E < 650 kV/cm \end{cases} \qquad (3)$$

where E is the electric field in kV/cm.

The bias dependence of the primary photocurrents is obtained by switching off the ionization process in the model and is shown by the green lines in Fig. 2(a). The actual avalanche multiplication is obtained by taking the difference between the measured photocurrent and the simulated primary photocurrent from Silvaco TCAD as shown in Fig. 2(b).

The α and β from Eqs. (2) and (3) for $Al_{0.75}Ga_{0.25}AsSb$ are shown in Fig. 3(a) together with data for AlAsSb [24] and $Al_{0.85}Ga_{0.15}As_{0.56}Sb_{0.44}$ [30]. Both α and β appear only marginally larger in $Al_{0.75}Ga_{0.25}AsSb$ when compared to $Al_{0.85}Ga_{0.15}As_{0.56}Sb_{0.44}$. Similar behavior has been reported in AlGaAs and AlGaInP lattice-matched to GaAs [38], in which the ionization coefficients do not vary significantly between alloys of high Al content. Figure 3(b) shows M_e-1 and M_h-1 from Fig. 2(a) plotted on a log-scale to emphasize the agreement of the simulated multiplication with experimental results over three orders of magnitude. Also shown are the multiplication curves obtained by using a random path length model [31] and the ionization
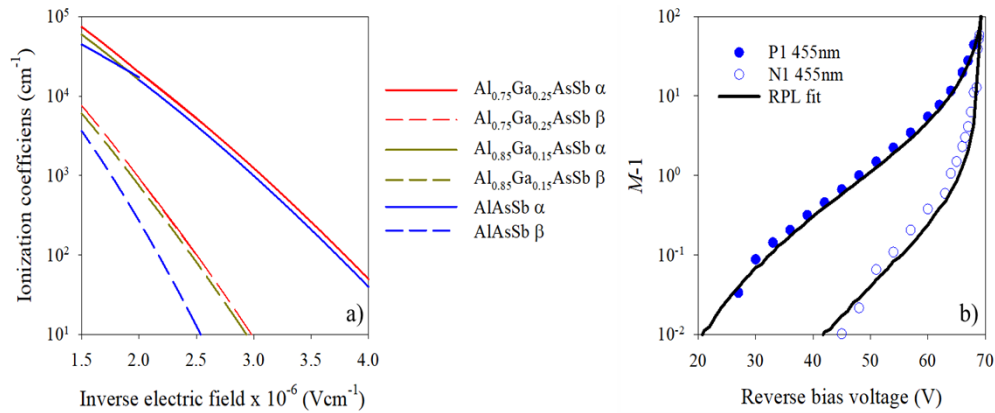
Fig. 3. a) Impact ionization coefficients for $Al_{0.75}Ga_{0.25}AsSb$, AlAsSb [24] and $Al_{0.85}Ga_{0.15}AsSb$ [30]. b) Multiplication data for P1 and N1 under pure injection conditions shown with data simulated by an RPL model, in the form $\log(M\text{-}1)$.
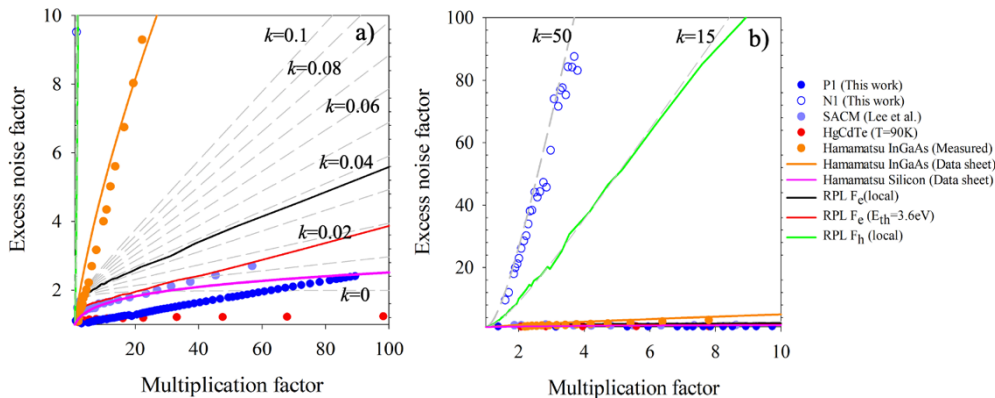

Fig. 4. a) Excess noise for P1 compared with a Hamamatsu Silicon device [6] a Hamamatsu InGaAs/InP device [39], a HgCdTe [12] device, and an $Al_{0.85}Ga_{0.15}As_{0.56}Sb_{0.44}$ SACM APD [22]. b) Excess noise for N1, shown on a different scale due to the much higher noise. Dashed lines in (a) are the excess noise predicted by McIntyre's local model for $k = 0$ to 0.1 in step of 0.01. Long dash and medium dash line in Fig. 4(b) represents McIntyre's local model for $k = 15$ and 50. Predicted excess noise data for N1 and P1 using a local model and an RPL model with a hard ionization threshold energy of $3.6\,eV$ are also shown.

coefficients with accurate knowledge of the electric field profiles in the structures investigated (including the background doping in the intrinsic region and depletion into the doped cladding layers). The impact ionization coefficients were assumed to be a function only of the local electric field (meaning that dead-space effects are not considered) in the structures. Excellent agreement can be seen between the experimental results and the simulation over three orders of magnitude.

The excess noise measurements were performed using the TIA-based system of Lau *et al.* [40], at a centre frequency of 10 MHz with illumination from the 455 nm LED. The excess noise measured under pure electron injection conditions in P1 (F_e) has sub-McIntyre characteristics with F remaining below the $k = 0$ limit of 2 up to $M > 60$, and then increasing linearly to $F = 2.45$ at $M = 90$. This excess noise is shown in Fig. 4(a) together with measurements on a Hamamatsu InGaAs/InP APD at 1550 nm [39]. Figure 4(a) also shows the excess noise obtained in a recently reported $Al_{0.85}Ga_{0.15}As_{0.56}Sb_{0.44}$ SACM-APD [22], in a HgCdTe APD [12] operating at 90 K

and a Hamamatsu silicon device [6]. The excess noise shown in this work is ~10 times lower than a commercially available InGaAs/InP SACM-APD [39] at $M = 30$ and is ~32% lower than that reported in the $Al_{0.85}Ga_{0.15}As_{0.56}Sb_{0.44}$ device [22]. It is even lower than the excess noise reported for good low noise commercial silicon APDs operating at ~420 nm for $M < 90$ whilst having a much lower operating voltage. Combined with an InGaAs or GaAsSb absorber, the $Al_{0.75}Ga_{0.25}AsSb$ should not only give the lowest excess noise reported SWIR SACM-APD at room temperature to date, but it can potentially work as a better low noise APD in the visible-NIR with a reach through design than most commercial silicon APDs.

4. Discussion

The exact mechanism responsible for the reduction in F relative to $Al_{0.85}Ga_{0.15}As_{0.56}Sb_{0.44}$ is as yet unclear. It may be due to the thicker avalanching region (1500 nm) and hence lower electric fields in the $Al_{0.75}Ga_{0.25}AsSb$ devices measured in this work, but it may be also related to the shape of the ionization probability density function (PDF) in this alloy. Recently, Lewis *et al.* [29] showed that $Al_{0.85}Ga_{0.15}As_{0.56}Sb_{0.44}$ gives rise to lower excess noise than predicted by the α/β ratio alone due to the non-exponential Weibull-Fréchet ionization PDF. A more 'peaked' ionization PDF may also exist in $Al_{0.75}Ga_{0.25}As_{0.56}Sb_{0.44}$ which may explain this even lower excess noise. Excess noise measurements with pure hole injection in N1 gives an extremely high F of 90 at $M = 4$ (F_h Fig. 4(b)), with an equivalent effective k_{eff} of 50. Neither a 'local' model [31] or an RPL model incorporating a 'hard' dead-space can simulate the excess noise behavior in the $Al_{0.75}Ga_{0.25}AsSb$ alloy for P1 or N1 as shown in Fig. 4. A local model for F_e (black line in Fig. 4(a)) significantly overestimates the noise and even a hard threshold energy of $E_{th} = 3.6$ eV (red line) does not fit the experimental results. A local model for F_h (effectively the noise due to the α/β ratio) predicts a much lower excess noise in N1 as shown by the green line in Fig. 4(b) and including any dead-space effects will only reduce this excess noise further, making the difference with experiments even larger. Ongoing work on the extraction of the Weibull-Fréchet ionization PDF in this alloy is made more complicated by the presence of the background doping and non-constant electric field. Impressively, this material shows comparable excess noise ($F \leq 1.3$ up to $M = 20$) at room temperature to that observed in HgCdTe [12] at $T = 90$ K. This suggests that $Al_{0.75}Ga_{0.25}AsSb$ may be used to produce ultra-low noise devices with performance which has not been previously achieved without cooling.

Disclosures. The authors declare no conflict of interest.

Data availability. Data underlying the results presented in this paper are available from Baolai Liang (bliang@cnsi.ucla.edu) and John David (j.p.david@sheffield.ac.uk) upon reasonable request.

References

1. U. N. Singh, T. F. Refaat, S. Ismail, K. J. Davis, S. R. Kawa, R. T. Menzies, and M. Petros, "Feasibility study of a space-based high pulse energy 2 μm CO2 IPDA lidar," Appl. Opt. **56**(23), 6531–6547 (2017).
2. Paul F. McManamon, *LiDAR Technologies and Systems* (SPIE, 2019).
3. S. M. Sze, *Physics of Semiconductor Devices*. (Wiley-Blackwell, 2006).
4. R. J. McIntyre, "Multiplication noise in uniform avalanche diodes," IEEE Trans. Electron Devices **ED-13**(1), 164–168 (1966).
5. R. B. Emmons, "Avalanche-Photodiode Frequency Response," J. Appl. Phys. **38**(9), 3705–3714 (1967).

6. Hamamatsu, *Hamamatsu Product Data Sheet (Silicon APD S16453 Short Wavelength Type APD)* (2018).

7. J. Michel, J. Liu, and L. C. Kimerling, "High-performance Ge-on-Si photodetectors," Nat. Photonics **4**(8), 527–534 (2010).

8. J. Campbell, "Evolution of Low-Noise Avalanche Photodetectors," IEEE J. Sel. Top. Quantum Electron. **28**(2: Optical Detectors), 1–11 (2022).

9. B. Wang, Z. Huang, Y. Yuan, D. Liang, X. Zeng, M. Fiorentino, and R. G. Beausoleil, "64 Gb/s low-voltage waveguide SiGe avalanche photodiodes with distributed Bragg reflectors," Photonics Res. **8**(7), 1118–1123 (2020).

10. L. J. J. Tan, J. S. Ng, C. H. Tan, and J. P. R. David, "Avalanche noise characteristics in submicron InP diodes," IEEE J. Quantum Electron. **44**(4), 378–382 (2008).

11. Y. L. Goh, A. R. J. Marshall, D. J. Massey, J. S. Ng, C. H. Tan, M. Hopkinson, J. P. R. David, S. K. Jones, C. C. Button, and S. M. Pinches, "Excess avalanche noise in In0.52Al0.48As," IEEE J. Quantum Electron. **43**(6), 503–507 (2007).

12. G. Finger, F. Eisenhauer, R. Genzel, C. Mandla, I. Baker, D. Alvarez, A. Amorim, W. Brandner, C. Dupuy, C. Deen, D. Ives, L. Mehrgan, M. Meyer, K. Perraut, G. Perrin, J. Stegmeier, C. Straubmeier, H. J. Weller, and V. Isgar, "Scientific detector workshop 2022 on-sky performance verification of near-infrared e−APD technology for wavefront sensing and demonstration of e−APD pixel performance to improve the sensitivity of large science focal planes," Astron. Nachrichten e20230069 (2023).

13. L. Zhu, H. Guo, Z. Deng, L. Yang, J. Huang, D. Yang, Z. Zhou, C. Shen, L. Chen, C. Lin, and B. Chen, "Temperature-Dependent Characteristics of HgCdTe Mid-Wave Infrared E-Avalanche Photodiode," IEEE J. Sel. Top. Quantum Electron. **28**(2: Optical Detectors), 1–9 (2022).

14. L. Zhu, H. Ge, H. Guo, L. Chen, C. Lin, and B. Chen, "Gain and Excess Noise in HgCdTe e-Avalanche Photodiodes at Various Temperatures and Wavelengths," IEEE Trans. Electron Devices **70**(5), 2384–2388 (2023).

15. P. J. Ker, A. R. J. Marshall, J. P. R. David, and C. H. Tan, "Low noise high responsivity InAs electron avalanche photodiodes for infrared sensing," Phys. Status Solidi C **9**(2), 310–313 (2012).

16. M. Ren, S. J. Maddox, M. E. Woodson, Y. Chen, S. R. Bank, and J. C. Campbell, "AlInAsSb separate absorption, charge, and multiplication avalanche photodiodes," Appl. Phys. Lett. **108**(19), 191108 (2016).

17. A. H. Jones, S. D. March, S. R. Bank, and J. C. Campbell, "Low-noise high-temperature AlInAsSb/GaSb avalanche photodiodes for 2-μm applications," Nat. Photonics **14**(9), 559–563 (2020).

18. A. A. Dadey, J. A. McArthur, A. Kamboj, S. R. Bank, D. Wasserman, and J. C. Campbell, "High-gain low-excess-noise MWIR detection with a 3.5-μm cutoff AlInAsSb-based separate absorption, charge, and multiplication avalanche photodiode," APL Photonics **8**(3), 36101 (2023).

19. X. Collins, B. White, Y. Cao, T. Osman, J. Taylor-Mew, J. S. Ng, and C. H. Tan, "Low-noise AlGaAsSb avalanche photodiodes for 1550 nm light detection," in (SPIE-Intl Soc Optical Eng, 2022), p. 16.

20. X. Collins, B. Sheridan, D. Price, Y. Cao, T. Blain, J. S. Ng, C. H. Tan, and B. White, "Low-noise AlGaAsSb avalanche photodiodes for 1550 nm light detection," Proc. SPIE **12417**, 124170K (2023).

21. Y. Cao, T. Osman, E. Clarke, P. K. Patil, J. S. Ng, and C. H. Tan, "A GaAsSb/AlGaAsSb Avalanche Photodiode with a very small Temperature Coefficient of Breakdown Voltage," J. Lightwave Technol. **40**(14), 4709–4713 (2022).

22. S. Lee, X. Jin, H. Jung, H. Lewis, Y. Liu, B. Guo, S. H. Kodati, M. Schwartz, C. Grein, T. Ronningen, J. Campbell, J. David, and S. Krishna, "High Gain, Low Noise, Room Temperature 1550 nm GaAsSb/AlGaAsSb Avalanche Photodiodes," Optica **10**(2), 147 (2023).

23. Y. Cao, T. Blain, J. D. Taylor-Mew, L. Li, J. S. Ng, and C. H. Tan, "Extremely low excess noise avalanche photodiode with GaAsSb absorption region and AlGaAsSb avalanche region," Appl. Phys. Lett. **122**(5), 51103 (2023).

24. X. Yi, S. Xie, B. Liang, L. W. Lim, X. Zhou, M. C. Debnath, D. L. Huffaker, C. H. Tan, and J. P. R. David, "Demonstration of large ionization coefficient ratio in AlAs0.56Sb0.44 lattice matched to InP," Sci. Rep. **8**(1), 9107–9113 (2018).

25. X. Yi, S. Xie, B. Liang, L. W. Lim, J. S. Cheong, M. C. Debnath, D. L. Huffaker, C. H. Tan, and J. P. R. David, "Extremely low excess noise and high sensitivity AlAs0.56Sb0.44 avalanche photodiodes," Nat. Photonics **13**(10), 683–686 (2019).

26. S. Lee, S. H. Kodati, B. Guo, A. H. Jones, M. Schwartz, M. Winslow, C. H. Grein, T. J. Ronningen, J. C. Campbell, and S. Krishna, "Low noise Al0.85Ga0.15As0.56Sb0.44avalanche photodiodes on InP substrates," Appl. Phys. Lett. **118**(8), 081106 (2021).

27. S. Lee, B. Guo, S. H. Kodati, H. Jung, M. Schwartz, A. H. Jones, M. Winslow, C. H. Grein, T. J. Ronningen, J. C. Campbell, and S. Krishna, "Random alloy thick AlGaAsSb avalanche photodiodes on InP substrates," Appl. Phys. Lett. **120**(7), 071101 (2022).

28. J. Taylor-Mew, V. Shulyak, B. White, C. H. Tan, and J. S. Ng, "Low Excess Noise of Al0.85Ga0.15As0.56Sb0.44avalanche Photodiode from Pure Electron Injection," IEEE Photonics Technol. Lett. **33**(20), 1155–1158 (2021).

29. H. I. J. Lewis, X. Jin, B. Guo, S. Lee, H. Jung, S. H. Kodati, B. Liang, S. Krishna, D. S. Ong, J. C. Campbell, and J. P. R. David, "Anomalous excess noise behavior in thick Al0.85Ga0.15As0.56Sb0.44 avalanche photodiodes," Sci. Rep. **13**(1), 9936 (2023).

30. B. Guo, X. Jin, S. Lee, S. Z. Ahmed, A. H. Jones, X. Xue, B. Liang, H. I. J. Lewis, S. H. Kodati, D. Chen, T. J. Ronningen, C. H. Grein, A. W. Ghosh, S. Krishna, J. P. R. David, and J. C. Campbell, "Impact Ionization Coefficients

of Digital Alloy and Random Alloy Al0.85Ga0.15As0.56Sb0.44 in a Wide Electric Field Range," J. Lightwave Technol. **40**(14), 4758–4764 (2022).

31. D. S. Ong, K. F. Li, G. J. Rees, J. P. R. David, and P. N. Robson, "A simple model to determine multiplication and noise in avalanche photodiodes," J. Appl. Phys. **83**(6), 3426–3428 (1998).

32. M. M. Hayat, W. L. Sargeant, and B. E. A. Saleh, "Effect of Dead Space on Gain and Noise in Si and GaAs Avalanche Photodiodes," IEEE J. Quantum Electron. **28**(5), 1360–1365 (1992).

33. H. Xu, E. W. Iverson, C.-C. Liao, K. Y. Cheng, and M. Feng, "Composition-Graded AlInP/AlGaAsSb/InP Type-II DHBTs With fT/fMAX = 450/510 GHz," IEEE Electron Device Lett. **34**(1), 33–35 (2013).

34. H. Jung, S. Lee, Y. Liu, X. Jin, J. P. R. David, and S. Krishna, "High electric field characteristics of GaAsSb photodiodes on InP substrates," Appl. Phys. Lett. **122**(22), 221102 (2023).

35. X. Zhou, S. Zhang, J. P. R. David, J. S. Ng, and C. H. Tan, "Avalanche Breakdown Characteristics of Al1–xGaxAs0.56Sb0.44 Quaternary Alloys," IEEE Photonics Technol. Lett. **28**(22), 2495–2498 (2016).

36. M. H. Woods, W. C. Johnson, and M. A. Lampert, "Use of a Schottky barrier to measure impact ionization coefficients in semiconductors," Solid-State Electron. **16**(3), 381–394 (1973).

37. A. G. Chynoweth, "Ionization Rates for Electrons and Holes in Silicon," Phys. Rev. **109**(5), 1537–1540 (1958).

38. H. I. J. Lewis, L. Qiao, J. S. Cheong, A. N. A. P. Baharuddin, A. B. Krysa, B. K. Ng, J. E. Green, and J. P. R. David, "Impact Ionization Coefficients in (AlxGa1-x)0.52In0.48P and AlxGa1-xAs Lattice-Matched to GaAs," IEEE Trans. Electron Devices **68**(8), 4045–4050 (2021).

39. Hamamatsu, *Hamamatsu Product Datasheet: InGaAs APD (G14858-0020AA)* (2010).

40. K. S. Lau, C. H. Tan, B. K. Ng, K. F. Li, R. C. Tozer, J. P. R. David, and G. J. Rees, "Excess noise measurement in avalanche photodiodes using a transimpedance amplifier front-end," Meas. Sci. Technol. **17**(7), 1941–1946 (2006).